PAPER

Generation of Various Types of Spatio-Temporal Phenomena in Two-Layer Cellular Neural Networks

Zonghuang YANG[†a)], *Student Member*, Yoshifumi NISHIO[††], *Member, and* Akio USHIDA[††], *Fellow*

SUMMARY The paper discusses the spatio-temporal phenomena in autonomous two-layer Cellular Neural Networks (CNNs) with mutually coupled templates between two layers. By computer calculations, we show how pattern formations, autowaves and classical waves can be regenerated in the networks, and describe the properties of these phenomena in detail. In particular, we focus our discussion on the necessary conditions for generating these spatio-temporal phenomena. In addition, the influences of the template parameters and initial state conditions of CNNs on the spatio-temporal phenomena are investigated.
key words: two-layer CNN array, reaction-diffusion equation, pattern formation, autowave, classical wave

1. Introduction

Studies of dynamic phenomena in arrays composed of oscillatory [1]–[7] and chaotic elements [8]–[18] are very important for understanding the phenomena observed in natural fields. A Cellular Neural Network (CNN) is a locally connected network [19], in which each cell is connected only to its neighbor, so the CNN allows efficient VLSI implementation of an analogue array-computing machine [20]–[24]. Because of its extraordinary computational power, the CNN is an ideal tool for the simulation of various spatio-temporal dynamics in discrete space.

Since the mid-1990s, investigations into the spatio-temporal dynamics in cellular neural networks have been widely carried out, and many papers have been published [5]–[18]. They have discussed the pattern formations and various autowaves such as excitability waves, concentration waves and so on, as observed in many fields such as biology, physics and chemistry. To date, these CNN arrays, composed of chaotic circuits [9]–[18] or second-order nonlinear circuits obtained by appropriately "reducing" Chua's circuit [8], have been examined for the generation of the above phenomena. In these studies, CNNs are used to approximate various nonlinear partial differential equations, particularly the well-known reaction-diffusion equations that show the Turing pattern and propagation phenomena in various continuous media [25]. In [5]–[7], Arena and coworkers and Manganaro et al. conducted studies on some other travelling

waves and self-organization phenomena in two-layer CNNs under the condition that the CNN cell exhibits slow-fast dynamics. This condition is so rigorous that the CNN places restrictions on other applications.

The objective of this work is to study spatio-temporal phenomena occurring in the mutually coupled two-layer CNNs, based on the CNN temporal eigenvalues. The two-layer CNNs possess a simpler structure, compared with the previously studied CNNs [8], [18]. We found from numerical simulations that similar phenomena can also be observed in our two-layer CNNs under milder necessary conditions. In addition to some nonlinear spatio-temporal phenomena such as autowaves and pattern formations, we found that another class of dynamic phenomena – classical wave propagation phenomena observed everywhere – can be simulated as well in the two-layer CNNs. These types of propagation phenomena have the properties of reflection, permeation and superposition. In particular, the necessary conditions for generating these spatio-temporal phenomena are discussed.

This paper is organized as follows: In Sect. 2, we review the two-layer CNNs with mutually coupled templates between the two layers. In Sects. 3 and 4, we discuss various spatio-temporal phenomena in terms of the temporal eigenvalue of the mutually coupled two-layer CNNs. The necessary conditions for these phenomena are indicated by the use of a decoupling technique. Several simulations for interesting spatio-temporal phenomena are shown and described in detail. In addition, the influences of the parameters in the cloning templates on propagation phenomena are also investigated by employing numerical calculation.

2. Two-Layer CNN Architecture

First, we review the mutually coupled two-layer CNN [26]–[28] used for investigating spatio-temporal phenomena. The CNN is described on the basis of the well-known Chua-Yang CNNs.

The system equations are formulated by introducing two coupling templates $\mathbf{C}_1$ and $\mathbf{C}_2$. In this paper, we also assume that the two-layer CNNs are composed of two-dimensional M by N array structures as shown on the left-hand side in Fig. 1. Each cell in the array is denoted by $c(i, j)$, where (i, j) stands for the position of a cell in the array, for $1 \le i \le M$ and $1 \le j \le N$. The cell local coupling is shown on the right-hand side in Fig. 1. Each cell has two state variables $x_{1,ij}$ and $x_{2,ij}$, where the subscripts 1 and 2 denote the first layer and the second layer of the two-
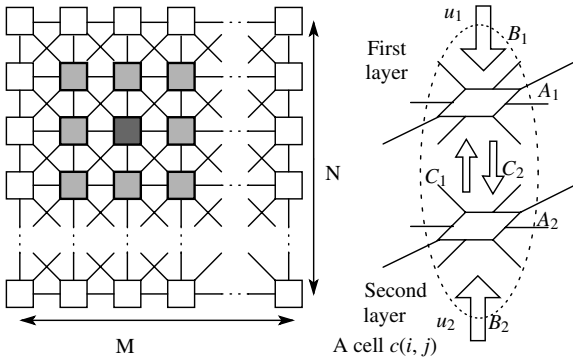
Fig. 1 A two-dimensional cellular neural network and a cell linked to neighbor cells with various templates.

layer CNN array. The state equations of the cell are given by two first-order differential equations given by Eq. (1), and the output equations are given by Eq. (2), where $f(\cdot)$ is a piecewise-linear nonlinear function defined by Eq. (3). The variables u and y refer to the input and the output variables of the cell, respectively. r is the coupling radius [19]. $N_r(i, j)$ denotes the neighbor cells of radius r of a cell $c(i, j)$. $A(i, j; k, l)$, $B(i, j; k, l)$, $C(i, j; k, l)$ and I denote the feedback coefficient, control coefficient, coupling coefficient between layers and bias current, respectively.

$$
\left.
\begin{aligned}
\frac{dx_{1,ij}}{dt} =\,& -x_{1,ij} + I_1 \\
& + \sum_{c(k,l)\in N_r(i,j)} A_1(i, j; k, l)y_{1,kl} \\
& + \sum_{c(k,l)\in N_r(i,j)} B_1(i, j; k, l)u_{1,kl} \\
& + \sum_{c(k,l)\in N_r(i,j)} C_1(i, j; k, l)y_{2,kl} \\
\frac{dx_{2,ij}}{dt} =\,& -x_{2,ij} + I_2 \\
& + \sum_{c(k,l)\in N_r(i,j)} A_2(i, j; k, l)y_{2,kl} \\
& + \sum_{c(k,l)\in N_r(i,j)} B_2(i, j; k, l)u_{2,kl} \\
& + \sum_{c(k,l)\in N_r(i,j)} C_2(i, j; k, l)y_{1,kl}
\end{aligned}
\right\}
\tag{1}
$$

$$
\left.
\begin{aligned}
y_{1,ij} = f(x_{1,ij}) \\
y_{2,ij} = f(x_{2,ij})
\end{aligned}
\right\}
\tag{2}
$$

$$
f(x) = 0.5(|x + 1| - |x - 1|). \tag{3}
$$

When $r = 1$, the CNN cloning templates [19] $\mathbf{A}_1$, $\mathbf{A}_2$, $\mathbf{B}_1$, $\mathbf{B}_1$, $\mathbf{C}_1$ and $\mathbf{C}_2$ are 3 times 3 matrices, which can be described to have a similar form as that of (4).

$$
\begin{pmatrix}
A(i,j;i-1,j-1) & A(i,j;i-1,j) & A(i,j;i-1,j+1) \\
A(i,j;i,j-1) & A(i,j;i,j) & A(i,j;i,j+1) \\
A(i,j;i+1,j-1) & A(i,j;i+1,j) & A(i,j;i+1,j+1)
\end{pmatrix}
\tag{4}
$$

The CNN is efficient for image processing applications such as center point detection, skeletonization, and so forth, which have been reported in our previous studies [26]–[28]. In the following sections, we discuss the spatio-temporal phenomena in the two-layer CNN.

3. Pattern Formations and Active Propagation Phenomena

3.1 Common Mechanism

Many nonlinear reaction-diffusion partial differential equations (PDEs) [25] have been proven to generate various types of nonlinear spatio-temporal phenomena, such as pattern formations, autowaves and self-organization phenomena. The concept of reaction-diffusion CNNs has been formalized to reproduce similar behaviors in Ref. [14], because they are mathematically described by a discretized version of the following well-known system of nonlinear partial differential equations – reaction-diffusion equations:

$$
\frac{\partial \boldsymbol{u}}{\partial t} = \boldsymbol{f}(\boldsymbol{u}) + \boldsymbol{D}\nabla^2 \boldsymbol{u}, \tag{5}
$$

where $\boldsymbol{u} \in \mathbf{R}^m$ represents a vector of continuously changing spatial variables, $\boldsymbol{f}(\boldsymbol{u}) \in \mathbf{R}^m$ their kinetics governing the oscillation in an isolated point of a medium, and the last term represents diffusion. $\boldsymbol{D}$ is an $m \times m$ diagonal matrix, which describes the intensity of diffusive coupling between the components of $\boldsymbol{u}$, and

$$
\nabla^2 u_i = \frac{\partial^2 u_i}{\partial x^2} + \frac{\partial^2 u_i}{\partial y^2}, \qquad i = 1, 2, \cdots, m \tag{6}
$$

is the Laplacian operator in $\mathbf{R}^2$.

In order to use the two-layer CNNs to approximate the above reaction-diffusion equation, we consider the equation with $\boldsymbol{u} \in \mathbf{R}^2$ in finite space, and assume it to be as follows:

$$
\left.
\begin{aligned}
\dot{u}_1 = -u_1 + a_1 v_1 + c_1 v_2 + D_1 \nabla^2 v_1 \\
\dot{u}_2 = -u_2 + a_2 v_2 + c_2 v_1 + D_2 \nabla^2 v_2
\end{aligned}
\right\}
\tag{7}
$$

where a_1, a_2, c_1 and c_2 are parameters, D_1, D_2 are diffusion coefficients, and v is a nonlinear function of u defined by (3). By expanding the Laplacian operator in the discrete space, Eq. (7) can be written as:

$$
\left.
\begin{aligned}
\dot{u}_{1;ij} =\,& -u_{1;ij} + a_1 v_{1;ij} + c_1 v_{2;ij} \\
& + D_1(v_{1;i-1,j} + v_{1;i+1,j} \\
& + v_{1;i,j-1} + v_{1;i,j+1} - 4v_{1;ij}) \\
\dot{u}_{2;ij} =\,& -u_{2;ij} + a_2 v_{2;ij} + c_2 v_{1;ij} \\
& + D_2(v_{2;i-1,j} + v_{2;i+1,j} \\
& + v_{2;i,j-1} + v_{2;i,j+1} - 4v_{2;ij})
\end{aligned}
\right\}
\tag{8}
$$

where $1 \le i \le M$ and $1 \le j \le N$. Compared with Eq. (1), the state equation (8) presents a two-layer autonomous reaction-diffusion standard CNN. The cloning template of the two-layer CNN array is described as follows:

$$
\mathbf{A}_1 = \begin{pmatrix} 0 & D_1 & 0 \\ D_1 & -4D_1 + a_1 & D_1 \\ 0 & D_1 & 0 \end{pmatrix}, \ \mathbf{C}_1 = \begin{pmatrix} 0 & 0 & 0 \\ 0 & c_1 & 0 \\ 0 & 0 & 0 \end{pmatrix},
$$

$$
\mathbf{A}_2 = \begin{pmatrix} 0 & D_2 & 0 \\ D_2 & -4D_2 + a_2 & D_2 \\ 0 & D_2 & 0 \end{pmatrix}, \ \mathbf{C}_2 = \begin{pmatrix} 0 & 0 & 0 \\ 0 & c_2 & 0 \\ 0 & 0 & 0 \end{pmatrix},
$$

$$\mathbf{B}_1 = \mathbf{0}, \ \mathbf{B}_2 = \mathbf{0}, \ I_1 = 0, \ I_2 = 0. \tag{9}$$

If at least one of the temporal eigenvalues has a positive real part, the CNN constructed by the connection between diffusing cells will become unstable and produce the pattern formations or active propagation phenomena. The necessary condition is described by Eq. (10), which is directly derived from those conditions obtained from the Turing patterns in an array of coupled circuits [8]:

$$\left. \begin{array}{l} \dfrac{(a_1 - 1)}{D_1} + \dfrac{(a_2 - 1)}{D_2} > 0 \\[2mm] [(a_1 - 1)D_2 - (a_2 - 1)D_1]^2 > -4D_1 D_2 c_1 c_2 \end{array} \right\} \tag{10}$$

The above condition ensures that only the two-layer CNN array is unstable in the linear region. As time increases, due to the positive real-part temporal eigenvalues, the cell states enter into nonlinear regions (i.e., saturation region or partial saturation region). In [8], the general principle of pattern formation has been indicated. The key mechanism of pattern formation is based on two types of necessary conditions. In addition to condition (10), the second condition refers to the requirement for the isolated cell to have a unique, stable equilibrium point. The two necessary conditions mean that the above equilibrium is merely a solution to the CNN array, which corresponds to a homogeneous pattern, but it should become unstable upon introducing the diffusion between cells; the pattern will also correspond to some other equilibrium points that happen to be stable for the pattern formation. On the other hand, if the isolated cell has no stable equilibrium point, then it behaves as a nonlinear oscillator with a limit cycle for the active wave propagation. These behaviors concerning the isolated cell have been discussed in detail in Ref. [29].

3.2 Pattern Formations

In this and the next subsection, we investigate the spatiotemporal phenomena in the two-layer CNNs by applying the aforementioned necessary conditions. Some significant findings are shown from the analysis of simulations.

3.2.1 Checkerboard

Experiment 1: This experiment is carried out under a two-layer CNN array consisting of 20×20 cells. The initial states of both layers are initiated by random noise shown in Fig. 2(a). In this case, the zero-fixed boundary condition is adopted. Under the template:

$$\mathbf{A}_1 = \begin{pmatrix} 0 & -0.2 & 0 \\ -0.2 & 1.8 & -0.2 \\ 0 & -0.2 & 0 \end{pmatrix}, \ \mathbf{C}_1 = \begin{pmatrix} 0 & 0 & 0 \\ 0 & -1 & 0 \\ 0 & 0 & 0 \end{pmatrix},$$

$$\mathbf{A}_2 = \begin{pmatrix} 0 & 0.1 & 0 \\ 0.1 & 0.3 & 0.1 \\ 0 & 0.1 & 0 \end{pmatrix}, \ \mathbf{C}_2 = \begin{pmatrix} 0 & 0 & 0 \\ 0 & 1 & 0 \\ 0 & 0 & 0 \end{pmatrix},$$

$$\mathbf{B}_1 = \mathbf{0}, \ \mathbf{B}_2 = \mathbf{0}, \ I_1 = 0, \ I_2 = 0, \tag{11}$$

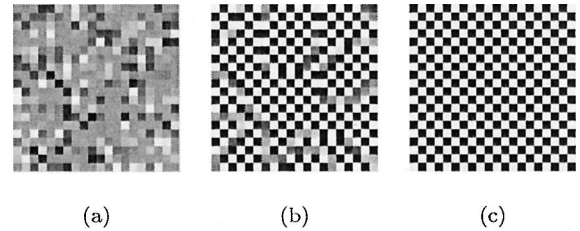we found a solution such that a stable output pattern with

Fig. 2 Checkerboard pattern formation in a two-layer CNN with random initial state condition. (a) is initial state, (b) is transient result, and (c) is steady output result.

the white-black grid alternating between the cells (so-called checkerboard) shown in Fig. 2(c) finally results in the first layer output of the CNN, where the states of all cells settle into the saturation region (i.e., each cell output is 1 or −1 corresponding to black or white, respectively).

Here, it should be emphasized that, the checkerboard pattern and stripe pattern formations in the next subsection can be obtained in a single-layer CNN array only with an infinite CNN structure [30]. Namely, a single-layer CNN with finite structure can only generate a defective checkerboard and stripe patterns, because the states of some cells, particularly near the boundary region, do not entirely enter into the saturation region. Note that the perfect checkerboard can be obtained in the two-layer CNN array with the finite structure. Moreover, we found that, irrespective of the initial states and the size of the array, the perfect checkerboard pattern can be obtained with the template parameter (11).

3.2.2 Stripe

Experiment 2: In this experiment, the procedure of stripe pattern formation is investigated. The CNN array consists of 100×100 cells with a zero-fixed boundary condition; its template is as follows:

$$\mathbf{A}_1 = \begin{pmatrix} 0 & 0.1 & 0 \\ 0.1 & 2.2 & 0.1 \\ 0 & 0.1 & 0 \end{pmatrix}, \ \mathbf{C}_1 = \begin{pmatrix} 0 & 0 & 0 \\ 0 & -1 & 0 \\ 0 & 0 & 0 \end{pmatrix},$$

$$\mathbf{A}_2 = \begin{pmatrix} 0 & 0.01 & 0 \\ 0.01 & 2.56 & 0.01 \\ 0 & 0.01 & 0 \end{pmatrix}, \ \mathbf{C}_2 = \begin{pmatrix} 0 & 0 & 0 \\ 0 & 1 & 0 \\ 0 & 0 & 0 \end{pmatrix},$$

$$\mathbf{B}_1 = \mathbf{0}, \ \mathbf{B}_2 = \mathbf{0}, \ I_1 = 0, \ I_2 = 0. \tag{12}$$

We observe that a stripe pattern formation occurs in the CNN, as shown in Fig. 3, where (a), (b) and (c) are respectively the initial state, the transient result and the steady output of the CNN. From the analysis of the simulation results, it is seen that the pattern formation process starts from the objects in the image (i.e., nonzero initial conditions), propagates around the objects, and generates new stripes with almost the same geometry as that of the original initiated objects. Then, it propagates again until the entire CNN array reaches the steady state. When the propagation wave front collides with another wave front or the boundary, the wave fronts eliminate each other without any interference or
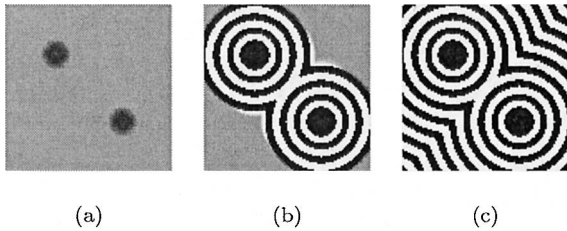
Fig. 3 Stripe pattern formation with $D_1 = 0.1$. (a) is initial state, (b) is transient result, and (c) is steady output result.
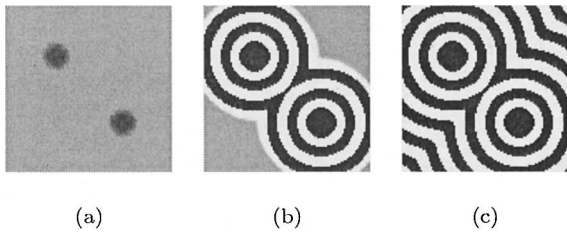

Fig. 4 Stripe pattern formation with $D_1 = 0.2$. (a) is initial state, (b) is transient result, and (c) is steady output result.

reflection.

Moreover, the density of the stripe pattern can be adjusted by suitably changing the template parameters. The simulation example is shown in Fig. 4, where the template is the same as (12) except that the diffusion coefficient D_1 is set to 0.2 instead of 0.1. Thus, the lower density stripe pattern formation is obtained.

From the above two simulation examples, we found that the shape of the stripe pattern is dependent on the initial state of the CNN array, and the density of the stripe pattern can be controlled by the template parameters. Thus, many interesting stripe patterns such as the coats of animals, fingerprints, and so forth may be regenerated by suitably selecting the initial conditions of the CNN array and the system parameters.

3.3 Active Propagation Phenomena

In this subsection, an investigation into active propagation phenomena is carried out in the two-layer CNN, which enables us to determine some basic properties of these phenomena. In the following experiment, an array of 100×100 cells is considered. Similarly, the selected parameters of the template satisfy the necessary condition (10) to guarantee the instability of the entire CNN with diffusion. Next, let us observe how the disturbance initiated inside the network propagates in the plane array.

Experiment 3: In this experiment, the initial condition is the same as in Experiment 2. The zero-flux boundary condition is adopted and the template is selected as follows:

$$\mathbf{A}_1 = \begin{pmatrix} 0 & 0.1 & 0 \\ 0.1 & 1.1 & 0.1 \\ 0 & 0.1 & 0 \end{pmatrix}, \mathbf{C}_1 = \begin{pmatrix} 0 & 0 & 0 \\ 0 & -1 & 0 \\ 0 & 0 & 0 \end{pmatrix},$$
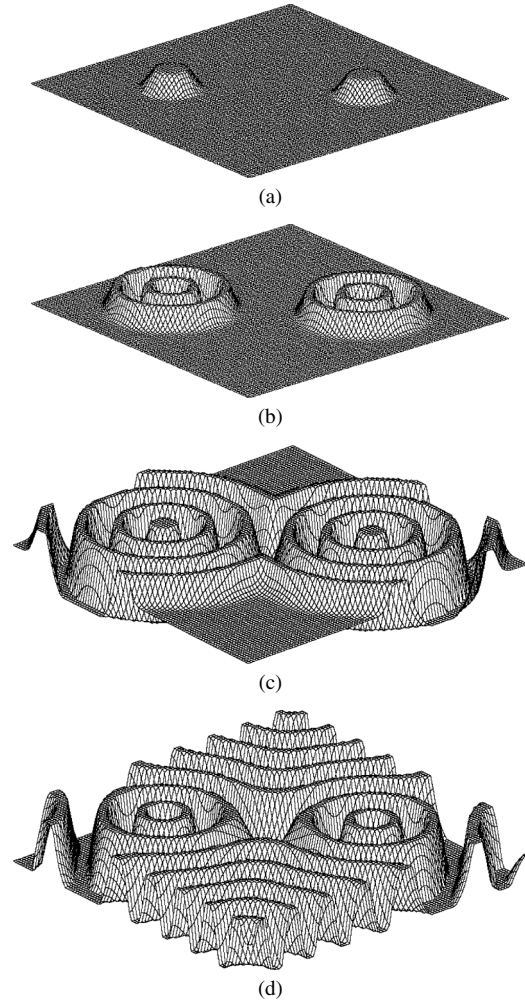

Fig. 5 A simulation for autowaves with two concentric circular waves. (a) is the initial state, (b), (c) and (d) show three snapshots obtained for different iterates.

$$\mathbf{A}_2 = \begin{pmatrix} 0 & -0.01 & 0 \\ -0.01 & 1.04 & -0.01 \\ 0 & -0.01 & 0 \end{pmatrix}, \mathbf{C}_2 = \begin{pmatrix} 0 & 0 & 0 \\ 0 & 1 & 0 \\ 0 & 0 & 0 \end{pmatrix},$$

$$\mathbf{B}_1 = \mathbf{0}, \mathbf{B}_2 = \mathbf{0}, I_1 = 0, I_2 = 0. \quad (13)$$

Figure 5 shows four snapshots of this simulation. The simulation result indicates that two concentric circular waves are generated. Their wave fronts propagate in all directions through the network from the initialized positions. Behind the wave fronts, the concentric waves centered at the cells where the process was initiated are visible. Moreover, they do not conserve energy but preserve amplitude and waveform, they are not reflected from obstacles but the colliding wave fronts are annihilated, and they do not produce any interference but diffract and pass around obstacles. Namely, this phenomenon is considered to be an autowave.

Note that we have used a simpler two-layer CNN array to reproduce the same phenomena with those observed in arrays made of chaotic cells [17], [18], and here the cell is merely a general nonlinear oscillator having a limit cycle, but does not exhibit slow-fast or chaotic dynamics. Simi-

larly, if we suitably adjust the diffusion coefficients D_1 or D_2, we can control the wavelength and speed of the propagation.

4. Classical Wave Propagation

4.1 Necessary Condition

We have shown in Sect. 3 that the two-layer CNNs can reproduce the pattern formation and the active propagation phenomena. These CNNs have a common property in that at least one of the temporal eigenvalues of CNNs has a positive real part. Moreover, this property is also one of the necessary conditions for the binary image processing applications of the two-layer CNNs [30]. However, when all the temporal eigenvalues have zero or negative real parts, what happens in the CNNs? We examine the phenomena in this section.

Let us consider an autonomous two-layer CNN with mutual coupling between layers. The equation is described in the following form:

$$\left.\begin{array}{l} \dot{x}_{1,ij} = -x_{1,ij} + (a_1 + 1)y_{1,ij} + c_1 y_{2,ij} \\ \qquad + d_1 \nabla^2 y_{2,ij} \\ \dot{x}_{2,ij} = -x_{2,ij} + (a_2 + 1)y_{2,ij} + c_2 y_{1,ij} \\ \qquad + d_2 \nabla^2 y_{1,ij} \end{array}\right\} \qquad (14)$$

where a_1, a_2, c_1, c_2, d_1 and d_2 are parameters. By expanding the Laplacian operator in discrete form, and in comparison with Eq. (1), the two-layer CNN has the following template:

$$\mathbf{A}_1 = \begin{pmatrix} 0 & 0 & 0 \\ 0 & a_1 + 1 & 0 \\ 0 & 0 & 0 \end{pmatrix}, \quad \mathbf{C}_1 = \begin{pmatrix} 0 & d_1 & 0 \\ d_1 & -4d_1 + c_1 & d_1 \\ 0 & d_1 & 0 \end{pmatrix},$$

$$\mathbf{A}_2 = \begin{pmatrix} 0 & 0 & 0 \\ 0 & a_2 + 1 & 0 \\ 0 & 0 & 0 \end{pmatrix}, \quad \mathbf{C}_2 = \begin{pmatrix} 0 & d_2 & 0 \\ d_2 & -4d_2 + c_2 & d_2 \\ 0 & d_2 & 0 \end{pmatrix},$$

$$\mathbf{B}_1 = \mathbf{0}, \ \mathbf{B}_2 = \mathbf{0}, \ I_1 = 0, \ I_2 = 0. \qquad (15)$$

If we assume that all the cells remain in the linear region, then the state equation (14) can be written as follows:

$$\left.\begin{array}{l} \dot{x}_{1,ij} = a_1 x_{1,ij} + c_1 x_{2,ij} + d_1 \nabla^2 x_{2,ij} \\ \dot{x}_{2,ij} = a_2 x_{2,ij} + c_2 x_{1,ij} + d_2 \nabla^2 x_{1,ij}. \end{array}\right\} \qquad (16)$$

Thus, the above linear differential equation can be solved by decoupling it into MN-decoupled systems of two first-order linear differential equations, and considering the MN orthonormal space-dependent eigenfunction $\phi_{MN}(m, n; i, j)$ of the discrete Laplacian operator, it can be assumed for almost all boundary conditions that:

$$\nabla^2 \phi_{MN}(m, n; i, j) = -k_{mn}^2 \phi_{MN}(m, n; i, j), \qquad (17)$$

where M and N are the CNN dimensions, m and n are the summation indexes for the current space variables i and j ($i = 0, 1, \cdots, M - 1$; $j = 0, 1, \cdots, N - 1$), and k_{mn}^2 are the corresponding spatial eigenvalues. In particular, for the zero-flux boundary condition, the spatial eigenfunction and

eigenvalue can be assumed as follows:

$$\phi_{MN}(m, n; i, j) = \cos\frac{(2i+1)m\pi}{2M}\cos\frac{(2j+1)n\pi}{2N} \qquad (18)$$

and

$$k_{mn}^2 = 4\left(\sin^2\frac{m\pi}{2M} + \sin^2\frac{n\pi}{2N}\right). \qquad (19)$$

Then, the expected solution of Eq. (16) can be expressed as a weighted sum of the $M \times N$ orthogonal space dependent eigenfunctions $\phi_{MN}(m, n; i, j)$ in the following form:

$$\left.\begin{array}{l} x_{1,ij}(t) = \sum_{m=0}^{M-1}\sum_{n=0}^{N-1}(\alpha_{mn}e^{\lambda_{mn1}t} + \beta_{mn}e^{\lambda_{mn2}t})\phi_{MN}(m, n; i, j) \\ x_{2,ij}(t) = \sum_{m=0}^{M-1}\sum_{n=0}^{N-1}(\gamma_{mn}e^{\lambda_{mn1}t} + \delta_{mn}e^{\lambda_{mn2}t})\phi_{MN}(m, n; i, j) \end{array}\right\}$$

$$(20)$$

where α_{mn}, β_{mn}, γ_{mn}, δ_{mn} are constants depending on the initial conditions. λ_{mn1} and λ_{mn2} are the roots of the following characteristic equation (21), which are influenced by the spatial eigenvalue k_{mn}^2 corresponding to the spatial eigenfunction $\phi_{MN}(m, n; i, j)$.

$$\left|\lambda_{mn}\begin{pmatrix} 1 & 0 \\ 0 & 1 \end{pmatrix} - \begin{pmatrix} a_1 & c_1 - k_{mn}^2 d_1 \\ c_2 - k_{mn}^2 d_1 & a_2 \end{pmatrix}\right| = 0 \qquad (21)$$

and

$$\lambda_{mn}[k_{mn}^2] = \frac{1}{2}\Big[(a_1 + a_2)$$

$$\pm\sqrt{(a_1 - a_2)^2 + 4(k_{mn}^2 d_2 - c_2)(k_{mn}^2 d_1 - c_1)}\Big] \qquad (22)$$

Equation (20) is important because the cell states of the two-layer CNN are given as the time-dependent weighted sums of spatial eigenfunctions. We have discussed in Sect. 3 that, if at least one of the temporal eigenvalues has a positive real part, the two-layer CNNs can be used for modeling the active media for nonlinear phenomena such as pattern formation and autowaves. However, if all the temporal eigenvalues have a zero or negative real part, all the states of the CNN are in the linear region, which agrees with our assumption above. Thus, the CNNs have the properties of linear space, such as superposition. Therefore, we can also use this CNN to model the passive media with/without loss in linear space.

4.2 Classical Waves

In this subsection, we investigate the passive propagation phenomena with/without loss in two-layer CNNs. In order to compare these with the propagation phenomena (Experiments 2, 3) in active media, we adopt the same-sized array with the same initial states and boundary condition (zero-flux) in Experiment 4.

Experiment 4: In this experiment, we observe the propagation phenomena in a two-layer CNN with/without loss.
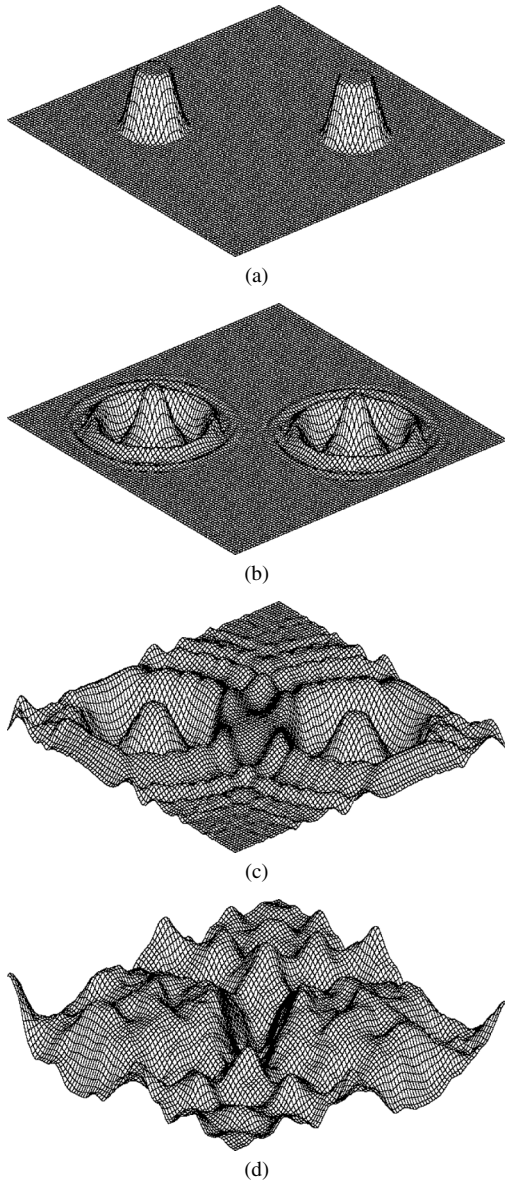
(a)

(b)

(c)

(d)

Fig. 6 A simulation for the passive wave propagation phenomenon without loss. (a) is the initial state, (b), (c) and (d) show three snapshots observed in different iterates.

Fig. 7 Graph of sum of State-Error Square vs. time for the passive wave propagation phenomenon without loss.

(a)

(b)

(c)

(d)

Fig. 8 A simulation for the passive wave propagation phenomenon with loss. (a) is the initial state, (b), (c) and (d) show snapshots observed in different iterates.

If we select the parameter set to satisfy that all the temporal eigenvalues of Eq. (20) have a zero real part, then the two-layer CNN will become a system without loss. This type of two-layer CNN can be used for modeling passive media without loss. For example, for the selected parameter set of $a_1 = 0$, $a_2 = 0$, $d_1 = -0.5$, $d_2 = 0.5$, $c_1 = -5$, and $c_2 = 5$, all the temporal eigenvalues of the CNN are complex numbers with a zero real part. The simulation result is shown in Fig. 6, where (a) is the initial state of the CNN and (b)–(d) are three snapshots obtained as time progresses.

The simulation result shows that the circular waves propagating from the initialized position are generated. These circular waves propagate in all directions through the plane array and their amplitudes decrease through propagation. When the waves collide with each other, they do not
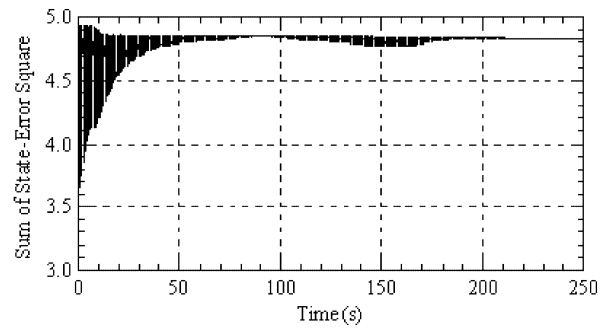
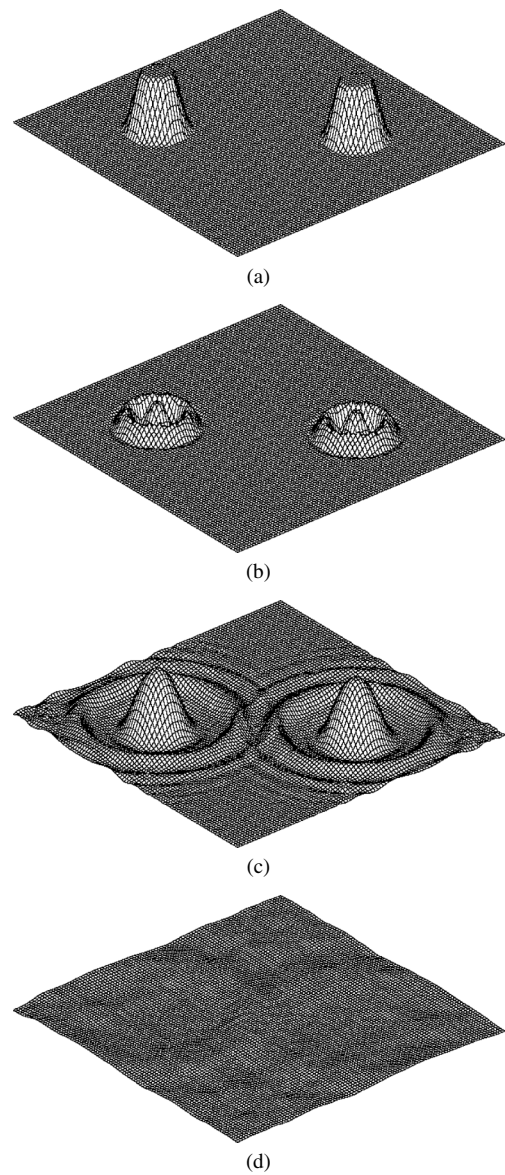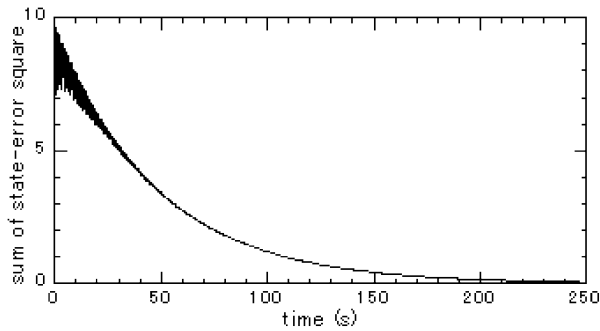**Fig. 9** Graph of sum of State-Error Square vs. time for the passive wave propagation phenomenon with loss.

annihilate and reflect, but permeate through and superpose on each other. When they collide with the boundary, the waves are reflected. Moreover, after the waves are repeatedly reflected and superposed, the initialized positions become invisible. These behaviors are similar to those of classical waves. The wave propagation continues forever due to the zero real part temporal eigenvalue. This dynamic process can be observed from the graph of the sum of State-Error Square versus the integration time shown in Fig. 7. The sum of State-Error Square is defined as:

$$S_{CNN}(t) = \sum_{i=1}^{M} \sum_{j=1}^{N} ((x_{1,ij}(t + \Delta t) - x_{1,ij}(t))^2$$
$$+ (x_{2,ij}(t + \Delta t) - x_{2,ij}(t))^2). \tag{23}$$

We can see from the graph that the sum of State-Error Square converges on a horizontal line with a value.

On the other hand, if we select the parameter set to satisfy all the temporal eigenvalues of the CNN having negative real parts, then each cell state will decay to zero, which can be derived from Eq. (20). This situation is suitable for the model of the passive media with loss. For example, if the parameters are set as $a_1 = -0.04$, $a_2 = 0$, $d_1 = -0.5$, $d_2 = 0.5$, $c_1 = -5$, and $c_2 = 5$, then all the temporal eigenvalues of the CNN will be complex numbers with a negative real part. Therefore, the CNN behaves as a damped system. The simulation result is shown in Fig. 8, where (a) shows the initial state of the CNN, and (b)–(d) show snapshots taken at three different times. From the simulation results, we can see that the propagation phenomenon has the same properties as the above loss-less system. However, the network is calm in the final due to the temporal eigenvalues having a negative real part. The dynamic process can be similarly demonstrated from the graph of sum of State-Error Square as shown in Fig. 9.

5. Conclusions

In this paper, we have shown that many types of spatio-temporal phenomena, such as pattern formation, autowaves and classical waves, can be reproduced in the two-layer CNNs with a simple structure. The conditions necessary for obtaining these phenomena have been indicated. The effects on propagation phenomena due to changes of system parameters have also been investigated. On the basis of our research results, we found that the two-layer CNN can be considered not only as a model of active media, but also as a model of passive media with/without loss. Moreover, it is worth mentioning that the type of two-layer CNN has a simpler structure compared with those arrays that consist of chaotic circuits or second-order nonlinear circuits. Although the pattern formations can be theoretically obtained in an infinite single-layer CNN array, applying the two-layer CNNs with an arbitrary number of cells to these problems enables us to obtain perfect pattern formations.

In addition, the two-layer CNNs described in this paper have zero B-templates. Thus, we can consider the C-template as a B-template in every layer, and mutually link one layer output with the other layer input. Therefore, it is possible to realize the above two-layer CNN Universal Machine (CNNUM) as a hardware simulator for simulating spatio-temporal phenomena, based on the current single-layer CNNUM chip. All these findings demonstrate that the two-layer CNNs have a real potential for a range of applications.

References

[1] T. Endo and S. Mori, "Mode analysis of a multimode ladder oscillator," IEEE Trans. Circuits Syst., vol.23, no.2, pp.100–113, 1976.

[2] T. Endo and S. Mori, "Mode analysis of two-dimensional low-pass multimode oscillator," IEEE Trans. Circuits Syst., vol.23, no.9, pp.517–530, 1976.

[3] T. Endo and S. Mori, "Mode analysis of a ring of a large number of mutually coupled van der Pol oscillators," IEEE Trans. Circuits Syst., vol.25, no.9, pp.7–18, 1978.

[4] M. Yamauchi, M. Wada, Y. Nishio, and A. Ushida, "Wave propagation phenomena of phase states in oscillators coupled by inductor as a ladder," IEICE Trans. Fundamentals, vol.E82–A, no.11, pp.2592–2598, Nov. 1999.

[5] P. Arena, S. Baglio, L. Fortuna, and G. Manganaro, "Self organization in two layer CNN," IEEE Trans. Circuits Syst., vol.45, no.2, pp.157–162, 1998.

[6] P. Arena, M. Branciforte, and L. Fortuna, "A CNN-based experimental frame for patterns and autowaves," Int. J. Circuit Theory Appl., vol.26, no.6, pp.635–650, 1998.

[7] G. Manganaro, P. Arena, and L. Fortuna, Cellular neural networks, Springer-Verlag, Berlin, Heidelberg, 1999.

[8] L. Goras and L.O. Chua, "Turing patterns in CNNs—Part I–III," IEEE Trans. Circuits Syst., vol.42, no.10, pp.602–637, 1995.

[9] L.O. Chua, "Special issue on nonlinear waves, patterns and spatio-temporal chaos in dynamic array," IEEE Trans. Circuits Syst., vol.42, no.10, pp.557–558, 1995.

[10] V.I. Nekorkin, V.B. Kazantsev, and L.O. Chua, "Chaotic attractors and waves in a one-dimensional array of modified Chua's circuits," Int. J. Bifurcation Chaos Appl. Sci. Eng., vol.6, no.7, pp.1295–1317, 1995.

[11] V.I. Nekorkin, V.B. Kazantsev, and M.G. Velarde, "Travelling waves in a circular array of Chua's circuits," Int. J. Bifurcation Chaos Appl. Sci. Eng., vol.6, no.3, pp.473–484, 1996.

[12] V.P. Munuzuri, V.P. Villar, and L.O. Chua, "Autowaves for image processing on a two-dimensional CNN array of excitable nonlinear circuits: Flat and wrinkled labyrinths," IEEE Trans. Circuits Syst., vol.40, no.3, pp.174–181, 1993.

[13] V.L. Zheleznyak and L.O. Chua, "Coexistence of low- and high-

dimensional spatiotemporal chaos in a chain of dissipatively coupled Chua's circuit," Int. J. Bifurcation Chaos Appl. Sci. Eng., vol.4, no.3, pp.639–674, 1994.

[14] L.O. Chua, M. Hasler, G.S. Mochytz, and J. Neirynck, "Autonomous cellular neural networks: A unified paradigm for pattern formation and active wave propagation," IEEE Trans. Circuits Syst., vol.42, no.10, pp.559–577, 1995.

[15] Y. Nishio and A. Ushida, "Spatio-temporal chaos in simple coupled chaotic circuits," IEEE Trans. Circuits Syst., vol.42, no.10, pp.678–686, 1995.

[16] M. Gilli, "Investigation of chaos in large arrays of Chua's circuits via a spectral technique," IEEE Trans. Circuits Syst., vol.42, no.10, pp.802–806, 1995.

[17] M.J. Ogorzalek, Z. Galias, A.M. Dabrowski, and W.R. Dabrowki, "Chaotic waves and spatio-temporal patterns in large arrays of doubly-coupled Chua's circuits," IEEE Trans. Circuits Syst., vol.42, no.10, pp.706–714, 1995.

[18] L. Pivka, "Autowave and spatio-temporal chaos in CNNs—Part I and II: A tutorial," IEEE Trans. Circuits Syst., vol.42, no.10, pp.638–663, 1995.

[19] L.O. Chua and L. Yang, "Cellular neural networks: Theory and applications," IEEE Trans. Circuits Syst., vol.35, no.10, pp.1257–1290, Oct. 1988.

[20] F. Werblin, T. Roska, and L.O. Chua, "The analogic cellular neural network as bionic eye," Int. J. Circuit Theory Appl., vol.23, no.6, pp.541–569, 1995.

[21] T. Roska and L.O. Chua, "The CNN universal machine," IEEE Trans. Circuits Syst., vol.40, no.3, pp.163–173, 1993.

[22] J.M. Cruz, L.O. Chua, and T. Roska, "A fast, complex and efficient test implementation of the CNN universal machine," Proc. 3rd Int. Workshop on Cellular Neural Networks and Their Applications, pp.61–66, Rome, 1994.

[23] S. Espejo, R. Carmona, R. Dominguez-Castro, and A. Rodriquez, "CNN universal chip in CMOS technology," Int. J. Circuit Theory Appl., vol.24, no.1, pp.93–111, 1996.

[24] L.O. Chua and T. Roska, "The CNN universal machine: An analogic array computer," IEEE Trans. Circuits Syst. II, vol.40, no.3, pp.163–173, 1993.

[25] J.D. Murray, Mathematical biology, Springer, Berlin, 1989.

[26] Z. Yang, Y. Nishio, and A. Ushida, "Image processing of two-layer CNNs—Applications and their stability," IEICE Trans. Fundamentals, vol.E85-A, no.9, pp.2052–2060, Sept. 2002.

[27] Z. Yang, Y. Nishio, and A. Ushida, "Templates and algorithms for two-layer cellular neural networks," Proc. 2002 International Joint Conference on Neural Networks, pp.1946–1951, Hawaii, USA, 2002.

[28] Z. Yang, Y. Nishio, and A. Ushida, "Characteristic of mutually coupled two-layer CNN and its stability," J. Circuits Syst. Comput., vol.12, no.4, pp.473–490, 2003.

[29] N. Takahashi and T. Nishi, "Complete stability analysis of cellular neural networks consisting of two cells," IEICE Technical Report, NLP2000-131, Feb. 2001.

[30] P. Thiran, K.R. Crounse, L.O. Chua, and M. Hasler, "Pattern formation properties of autonomous cellular neural networks," IEEE Trans. Circuits Syst., vol.42, no.10, pp.757–774, 1995.

Zonghuang Yang received the B.E. degree in Radio Engineering from South East University, Nanjing China in 1985, and the M.E. degree in Electrical and Electronic Engineering from Tokushima University, Tokushima, Japan, in 2001. He is currently working toward the Ph.D. degree in the same department of Tokushima University. His research interests include the theory and application of cellular neural networks.

Yoshifumi Nishio received the B.E., M.E., and Ph.D. degrees in Electrical Engineering from Keio University, Yokohama, Japan, in 1988, 1990, and 1993, respectively. In 1993, he joined the Department of Electrical and Electronic Engineering at Tokushima University, Tokushima, Japan, where he is currently an Associate Professor. From May 2000 he spent a year in the Laboratory of Nonlinear Systems (LANOS) at the Swiss Federal Institute of Technology Lausanne (EPFL), as a visiting professor. His research interests include analysis and application of chaos in electrical circuits, analysis of synchronization in coupled oscillators circuits, development of analyzing methods for nonlinear circuits and theory and application of cellular neural networks. Dr. Nishio is a member of the IEEE.

Akio Ushida received the B.E. and M.E. degrees in Electrical Engineering from Tokushima University in 1961 and 1966, respectively, and the Ph.D. degree in Electrical Engineering from University of Osaka Prefecture in 1974. He was an Associate Professor from 1973 to 1980 at Tokushima University. From 1980 to 2003, he was a Professor in the Department of Electrical and Electronic Engineering at Tokushima University. Since 2003, he has been with the Department of Mechanical-Electronic Engineering, Tokushima Bunri University. From 1974 to 1975 he spent one year as a visiting scholar at the Department of Electrical Engineering and Computer Sciences at the University of California, Berkeley. His current research interests include numerical methods and computer-aided analysis of nonlinear systems. Dr. Ushida is a member of the IEEE.